

## PERSISTENT X-RAY EMISSION FROM ASASSN-15LH: PRE-SLSN DENSE WIND?

YAN HUANG<sup>1,2</sup> AND ZHUO LI<sup>1,2</sup><sup>1</sup>Department of Astronomy, School of Physics, Peking University, Beijing 100871, China; hyan623@pku.edu.cn<sup>2</sup>Kavli Institute for Astronomy and Astrophysics, Peking University, Beijing 100871, China*Draft version May 9, 2019*

## ABSTRACT

The persistent soft X-ray emission at the location of the so-far most luminous supernova (SN), ASASSN-15lh (or SN 2015L), with  $L \sim 10^{42} \text{ erg s}^{-1}$ , is puzzling. We show that it can be explained by radiation from the SN-shock accelerated electrons inverse-Compton scattering the intense UV photons. In this interpretation, the circumstellar medium is derived to be a wind ( $n \propto R^{-2}$ ) with mass-loss rate of  $\dot{M} \gtrsim 3 \times 10^{-3} M_{\odot} (v_w/10^3 \text{ km s}^{-1}) \text{ yr}^{-1}$ , and the initial velocity of the bulk SN ejecta is  $\lesssim 0.02c$ . The non-detection in radio is naturally expected due to strong synchrotron self-absorption and free-free absorption in the dense medium. This constraint implies a strong wind ejected just within  $\sim 8(v_w/10^3 \text{ km s}^{-1})^{-1} \text{ yrs}$  before the explosion of ASASSN-15lh by its progenitor star.

*Subject headings:* stars: mass-loss - supernovae:general - SLSN: individual (ASASSN-15lh)

## 1. INTRODUCTION

Super-luminous supernovae (SLSNe) are a type of stellar explosions with a luminosity 10 or more times higher than the standard supernovae (SNe) (Gal-Yam 2012). SN 2005ap was the first discovered SLSN, with an absolute magnitude at peak around  $-22.7 \text{ mag}$  (Quimby et al. 2007). Over the past decade, due to the large field-of-view, rapid-cadence transient searches, more than a hundred SLSNe had been found (Quimby et al. 2007; Smith & McCray 2007; Gal-Yam 2012; Nicholl et al. 2014). SLSNe are likely associated with the deaths of the most massive stars, but the progenitors and the physics of the explosion are still not understood. Several power-input mechanisms have been proposed for SLSNe, including gamma-ray heating by the radioactive decays of  $^{56}\text{Ni}$  and  $^{56}\text{Co}$  (Gal-Yam et al. 2009), magnetar spin-down (Kasen & Bildsten 2010; Woosley 2010), SN shock interaction with dense material in the environment (Smith & McCray 2007; Chevalier & Irwin 2011), and the pair-instability SNe (Woosley et al. 2007; Woosley 2017). Unveiling the progenitors and explosion mechanisms of SLSNe are crucial for our understanding of massive star evolution.

ASASSN-15lh was discovered by the All-Sky Automated Survey for Supernovae (ASAS-SN) with absolute magnitude of  $-23.5$  and a peak bolometric luminosity of  $L_{\text{bol}} = (2.2 \pm 0.2) \times 10^{45} \text{ erg s}^{-1}$ , more than twice as previously known SLSNe, making it the most luminous SNe thus far (Dong et al. 2016). The temporary behavior showed a unique double-humped structure. It reached the primary peak at several tens days after explosion, and then decayed. However, a rebrightening began  $\simeq 90$  days after the primary peak and was followed by a long plateau (Godoy-Rivera et al. 2017). A persistent soft X-ray radiation with luminosity  $L \sim 10^{41} - 10^{42} \text{ erg s}^{-1}$  at the location of ASASSN-15lh are observed by Chandra/CXO during the follow-up campaign (Margutti et al. 2017). Radio follow-up of ASASSN-15lh had been carried out by ATCA, 197 days after first detection of optical obser-

vation, but no radio emission was detected (Kool et al. 2015).

The major features characteristics of ASASSN-15lh make it classified as a hydrogen-poor (type I) SLSN (Dong et al. 2016) (see, however, Leloudas et al. 2016; Krühler et al. 2017, who suggest that ASASSN-15lh is a tidal disruption event from a supermassive Kerr black hole). There are many discussion on the power source of it. Dong et al. (2016) suggest that the large radiation energy does not favor the radioactive decay and magnetar as main energy sources, and the lack of spectral feature also disfavors the model of interaction with dense medium. But (Metzger et al. 2015; Dai et al. 2016) suggest that the new updated magnetar models may still work. However the later observed rebrightening put new challenges. Chatzopoulos et al. (2016) explained the double-humped as a signature of the interaction of massive SN ejecta  $M_{\text{ej}} \approx 36 M_{\odot}$  with an H-poor circumstellar shell of  $M_{\text{CSM}} \approx 20 M_{\odot}$ .

If the X-ray emission is really produced by ASASSN-15lh, one may expect it varying with time, other than keeping a constant luminosity, so the interpretation of X-ray emission from the host galaxy is favored (Margutti et al. 2017). Here we show that the persistent behavior can be explained by radiation from the SN shock, i.e., the shock-accelerated electrons up-scattering the inner coming UV photons from the SN photosphere. In this way, the medium density can be derived, and gives hint of the progenitor of ASASSN-15lh. In §2, we give the main observational results of ASASSN-15lh. Our model is provided in §3, and §4 is results of modelling, followed by discussion and conclusion (§5). Notice that we use the  $q_x = q/10^x$  convention and the cgs units in the following unless stated otherwise.

## 2. OBSERVATIONS

ASASSN-15lh was discovered on 2015 June 14 (UT) by the ASAS-SN survey (Dong et al. 2016). The redshift is  $z = 0.2326$ , corresponding to a luminosity distance of  $d_L \simeq 1171 \text{ Mpc}$ . At the primary peak of the light curve the absolute magnitude is  $M_{V,AB} = -23.5 \pm 0.1$ , and the

TABLE 1  
OBSERVED X-RAY (0.3-10 KEV) FLUX FROM ASASSN-15lh,  
ASSUMING A POWER-LAW SPECTRUM WITH PHOTON INDEX  $\Gamma = 3$   
(MARGUTTI ET AL. 2017).

Date (MJD)	Exposure (ks)	Unabsorbed Flux (erg s <sup>-1</sup> cm <sup>-2</sup> )
57338	10	$< 2.0 \times 10^{-15}$
57369	10	$\sim 4.4 \times 10^{-15}$
57438	40	$\sim 3.6 \times 10^{-15}$
57619	30	$\sim 4.9 \times 10^{-15}$

bolometric luminosity is  $L_{\text{bol}} = (2.2 \pm 0.2) \times 10^{45} \text{ erg s}^{-1}$ . Because of similarities in temperature, luminosity and radius evolutions between ASASSN-15lh and the other SLSNe-I, ASASSN-15lh was characterized as hydrogen-poor SLSNe-I (Dong et al. 2016). The host galaxy of ASASSN-15lh is a luminous galaxy ( $M_K \simeq -25.5$ ) with little star formation.

The primary peak time is JD2457179 (June 05, 2015). (Godoy-Rivera et al. 2017) reports a UV rebrightening starts 90 days (observer frame) after the primary peak, is followed by a  $\simeq 120$  days long plateau in the bolometric light curve, and fades again since  $\simeq 210$  days after explosion. Over the  $\sim 550$  days since detection, ASASSN-15lh has radiated  $\sim 1.7 - 1.9 \times 10^{52} \text{ erg}$ .

Margutti et al. (2017) presents the detection of persistent soft X-ray emission, with luminosity  $L \sim 10^{41} - 10^{42} \text{ erg s}^{-1}$ , at the location of ASASSN-15lh as revealed by Chandra. They obtain 4 epochs of deep X-ray observations with the Chandra/X-ray Observatory (CXO) on November 12, 2015, December 13, 2015, February 20, 2016, and August 19, 2016, respectively, corresponding to 129.4 days, 154.6 days, 201.5 days and 357.8 days (rest frame), respectively, since optical maximum light on June 5, 2015. Table 1 shows the X-ray flux observed by CXO.

Kool et al. (2015) used ATCA to observe the radio emission, on November 21.1 UT, 2015, i.e., 197 days after the first detection of optical observation (MJD 57150.5). No radio emission was detected at the SN location. A  $3\sigma$  upper limit of  $23 \mu\text{Jy}$  at 5.5 GHz and  $21 \mu\text{Jy}$  at 9 GHz are given.

### 3. MODEL

#### 3.1. Hydrodynamic evolution

Consider that the SN ejecta of ASASSN-15lh drive a shock propagating into the circumstellar medium (CSM). The hydrodynamic evolution of the shock depends on the density structure of the freely expanding SN ejecta and the structure of the CSM. Consider the CSM to be a steady stellar wind released from the progenitor star of ASASSN-15lh. For a free wind with constant mass loss rate  $\dot{M}$  and wind speed  $v_w$ , one has the wind density as function of the radius  $R$

$$n = \frac{\dot{M}}{4\pi R^2 m_p v_w} \equiv AR^{-2}. \quad (1)$$

So  $A$  is a parameter representing the density of the wind like CSM. For a wind mass-loss rate of  $\dot{M} = 10^{-5} M_\odot \text{ yr}^{-1}$  and a wind speed of  $v_w = 10^8 v_{w,8} \text{ cm s}^{-1}$ , we obtain the typical value of  $A = 10^{35} A_{35} \text{ cm}^{-1}$ .

Consider a spherical SN ejecta to be homogeneous with a constant velocity  $\beta_0 c$  and a bulk kinetic energy  $E_0$ . Ini-

tially the shock expand with the initial velocity  $\beta = \beta_0$ , transferring the ejecta energy into the swept-up medium. The shock energy when the shock expands to radius  $R$  is

$$E = (\beta c)^2 \int_0^R n m_p 4\pi r^2 dr = 4\pi A m_p R (\beta c)^2. \quad (2)$$

When a half of the initial energy is transferred into the shocked medium,  $E = \frac{1}{2} E_0$ , the shock starts to decelerate significantly. This happens at the so-called deceleration radius

$$R_{\text{dec}} = \frac{E_0}{8\pi m_p A c^2 \beta_0^2} \approx 2.7 \times 10^{20} \text{ cm} E_{0,52} A_{35}^{-1} \beta_{0,-1}^{-2}. \quad (3)$$

For ASASSN-15lh, we normalize the initial energy to be  $E_0 = 10^{52} E_{0,52}$  since the radiated energy is order of  $10^{52} \text{ erg}$  (but the explosion energy could be even tens to hundreds times larger than the radiation energy (Walch & Naab 2015)). The corresponding deceleration time since the SN explosion is

$$t_{\text{dec}} = \frac{R_{\text{dec}}}{c\beta_0} \approx 2.8 \times 10^3 \text{ yr} E_{0,52} A_{35}^{-1} \beta_{0,-1}^{-3}. \quad (4)$$

Thus, at time  $t \leq t_{\text{dec}}$ , the shock propagates in a constant velocity,  $\beta = \beta_0$ , and the shock radius is  $R = c\beta_0 t$ . When  $t > t_{\text{dec}}$ , the shock dynamics transits into the self-similar Sedov-Taylor solution, then we have the shock velocity  $\beta = \beta_0^{2/3} (ct/R_{\text{dec}})^{-1/3}$ . Note, the sensitive dependence of  $t_{\text{dec}}$  on  $\beta_0$  implies that in our case of non-relativistic shock in ASASSN-15lh,  $\beta_0 \ll 1$ ,  $t_{\text{dec}}$  is much larger than the relevant observation time. So we actually only need to consider the free expanding phase of  $t < t_{\text{dec}}$  with  $\beta = \beta_0$ .

#### 3.2. Shock radiation

Given the hydrodynamic evolution of the SN shock, we next discuss the radiation from the shock. The swept-up CSM electrons will be accelerated by the shock, via, e.g., diffusive shock acceleration mechanism, and the post-shock magnetic field is also amplified, hence the accelerated electrons will give rise to synchrotron and inverse-Compton (IC) radiation in the downstream region (e.g., Chevalier & Fransson 2006). We discuss the IC and synchrotron components separately below, focussing on their contribution on X-ray and radio emission, respectively.

##### 3.2.1. IC radiation

We first show that for ASASSN-15lh, IC is the dominant cooling process other than synchrotron radiation for the accelerated electrons. The synchrotron cooling time of electrons with Lorentz factor (LF)  $\gamma_e$  is  $t_{\text{syn}} = 3m_e c / 4\sigma_T U_B \gamma_e$ , depending on the energy density of the post-shock magnetic field,  $U_B = 4\epsilon_B n m_p (\beta c)^2$ , where  $\epsilon_B$  is the equipartition parameter for magnetic field. On the other hand, the electrons will also lose energy by up-scattering the ambient photons. Given the intense UV photon emission from the inner photosphere of the newly exploded SN, a dominant contribution of the seed photons for IC scattering is the UV photons (Björnsson & Fransson 2004). For a UV luminosity of  $L_{\text{UV}}$ , the photon energy density at the shock region is  $U_{\text{ph}} = L_{\text{UV}} / 4\pi R^2 c$ , then the electron cooling

time due to IC scattering UV photons can be derived as  $t_{\text{IC}} = 3m_e c / 4\sigma_T U_{\text{ph}} \gamma_e$ . So the ratio of synchrotron to IC cooling time is

$$\frac{t_{\text{syn}}}{t_{\text{IC}}} = \frac{U_{\text{ph}}}{U_B} \approx 4.4 \times 10^3 L_{\text{UV},45} \epsilon_{B,-1}^{-1} A_{35}^{-1} \beta_{0,-1}^{-2}. \quad (5)$$

For ASASSN-15lh, given the large UV luminosity (Godoy-Rivera et al. 2017) we normalize the UV luminosity as  $L_{\text{UV}} = 10^{45} L_{\text{UV},45} \text{erg}$ . For  $\beta \ll 1$  and a wide range of  $A$ , one has  $t_{\text{syn}} \gg t_{\text{IC}}$ , hence we assume IC cooling dominates synchrotron cooling.

By diffusive shock acceleration theory, the CSM electrons swept-up by the SN shock are accelerated to follow a power law in momentum  $dN_e/dp_e \propto p_e^{-p}$  with  $p_e \geq p_{\text{min}}$  and  $p$  the power law index. For relativistic electrons we have  $p_e \propto \gamma_e$ , thus the electron distribution at  $\gamma_e \gtrsim 2$  can also be approximated as a power law in electron's LF with the same index,  $dN_e/d\gamma_e \propto \gamma_e^{-p}$ . Radio observations of Type Ib/c SNe indicate  $p \approx 3$  (Chevalier & Fransson 2006), thus we take  $p = 3$  here. This is also consistent with the poorly constrained X-ray spectrum of ASASSN-15lh (Margutti et al. 2017).

Define that the accelerated electrons carry a fraction  $\epsilon_e$  of the post-shock internal energy  $U = n_e m_p \beta^2 c^2$ , with  $n_e$  the postshock proton number density. We will take the typical value  $\epsilon_e = 0.1$ . If the bulk electrons are relativistic, then using the approximation of power-law in LF, the minimum LF can be derived to be  $\gamma_m = [(p-2)/(p-1)](m_p/m_e)\epsilon_e\beta^2$  (e.g., Piran et al. 2013). The minimum LF is a constant initially when the shock is not decelerated,  $\beta = \beta_0$ . However, if the initial shock velocity  $\beta_0$  is low enough, the bulk electrons may be non-relativistic,  $\gamma_{\text{min}} - 1 \lesssim 1$ . Since we are only interested in the electrons that emit synchrotron and IC radiation, the relevant electrons should be relativistic,  $\gamma_e \gtrsim 2$ . Thus, for the characteristic frequencies in the synchrotron and IC spectra, we should take

$$\gamma_m = \max\left(\frac{p-2}{p-1} \frac{m_p}{m_e} \epsilon_e \beta^2, 2\right). \quad (6)$$

If the bulk accelerated electrons are non-relativistic, the electron energy is, for  $p \leq 3$ , dominated by electrons with  $\gamma_e \gtrsim 2$  (Sironi & Giannios 2013), i.e., relativistic electrons. Thus, we can approximate  $\epsilon_e U \approx \int_2 \gamma_e m_e c^2 (dn_e/d\gamma_e) d\gamma_e$ . Moreover, the postshock electron number density for  $\gamma_e \geq 2$  is  $n_{\text{rel}} \approx \int_2 (dn_e/d\gamma_e) d\gamma_e$ . Combining these two equations gives the fraction of relativistic electrons,  $\gamma_e \geq 2$ , in the total electrons,

$$f_{\text{rel}} \equiv \frac{n_{\text{rel}}}{n_e} = \min\left(1, \frac{p-2}{p-1} \frac{m_p}{m_e} \frac{\epsilon_e \beta^2}{2}\right). \quad (7)$$

So given the total number of the shock swept-up electrons  $N_e = 4\pi AR$ , the relativistic electron number that give rise to synchrotron and IC radiation is only  $f_{\text{rel}} N_e$ .

The radiative cooling changes the electron distribution. Let the electron cooling time, dominated by IC cooling, equal the age of the SN shock,  $t_{\text{IC}} = t$ , we obtain the cooling LF  $\gamma_c = 3m_e c / 4\sigma_T U_{\text{ph}} t$ . For electrons with  $\gamma_e > \gamma_c$  the electrons cool significantly and the distribution deviates from the injection power law, with the index changed to  $p+1$ . Given the bright UV emission of ASASSN-15lh, we find that at the beginning  $\gamma_c < \gamma_m$ , all

electrons are in fast cooling regime. Later  $\gamma_c > \gamma_m$  may happen, thus we should consider both fast cooling and slow cooling regime in deriving the electron distribution and radiation spectrum.

Next we discuss the radiation spectrum from IC scattering UV photons, considering both fast and slow cooling cases, similar to Sari et al. (1998). On average, the IC radiation power of a single electron with  $\gamma_e$  is  $P_{\text{IC}} = (4/3)\sigma_T c \gamma_e^2 U_{\text{ph}}$ . For simplicity, we assume the seed photons are isotropic, neglecting the order of unity correction of anisotropic incoming photons. The UV photons are in a black body like spectrum, thus the energy distribution is narrow, and we can approximate them as monochromatic, with a frequency of  $\nu_0 = 3kT_{\text{BB}}/h$ , where the rest-frame temperature of the UV photons is  $T_{\text{BB}} \approx 2.0 \times 10^4 \text{K}$  (Dong et al. 2016).

Typically, the UV photons will be scattered by electrons with  $\gamma_e$  up to a frequency of  $\nu_s = (4/3)\gamma_e^2 \nu_0$ . The specific power at  $\nu_s$  is  $P_{\text{m,IC}} \approx P_{\text{IC}}/\nu_s = \sigma_T c U_{\text{ph}}/\nu_0$ , actually independent of  $\gamma_e$ . The relativistic electron number is  $f_{\text{rel}} N_e$ , and the observed IC flux at spectral peak is  $F_{\text{m,IC}} = f_{\text{rel}} N_e P_{\text{m,IC}} / 4\pi d_L^2$ , i.e.,

$$F_{\text{m,IC}} = 1.6 \times 10^{-2} \mu\text{Jy} A_{35} L_{\text{UV},45} t_d^{-1} d_{L,28}^{-2} \beta_{0,-1}^{-1} f_{\text{rel}}, \quad (8)$$

where  $t_d = t/1$  day. We take broken power law approximation for the radiation spectrum. For fast cooling case,  $\gamma_c < \gamma_m$ , the emergent IC spectrum is given by (Ghisellini 2013)

$$F_{\nu,\text{IC}} = \begin{cases} F_{\text{m,IC}} \left(\frac{\nu}{\nu_{s,c}}\right), & \nu < \nu_{s,c} \\ F_{\text{m,IC}} \left(\frac{\nu}{\nu_{s,c}}\right)^{-1/2}, & \nu_{s,c} \leq \nu \leq \nu_{s,m} \\ F_{\text{m,IC}} \left(\frac{\nu_{s,m}}{\nu_{s,c}}\right)^{-1/2} \left(\frac{\nu}{\nu_{s,m}}\right)^{-p/2}, & \nu > \nu_{s,m} \end{cases} \quad (9)$$

whereas for slow cooling case,  $\gamma_m < \gamma_c$ , the IC spectrum is

$$F_{\nu,\text{IC}} = \begin{cases} F_{\text{m,IC}} \left(\frac{\nu}{\nu_{s,m}}\right), & \nu < \nu_{s,m} \\ F_{\text{m,IC}} \left(\frac{\nu}{\nu_{s,m}}\right)^{-\frac{p-1}{2}}, & \nu_{s,m} \leq \nu \leq \nu_{s,c} \\ F_{\text{m,IC}} \left(\frac{\nu_{s,c}}{\nu_{s,m}}\right)^{-\frac{p-1}{2}} \left(\frac{\nu}{\nu_{s,c}}\right)^{-p/2}, & \nu > \nu_{s,c} \end{cases} \quad (10)$$

The break frequencies in the spectrum are relevant to the characteristic electron LFs as  $\nu_{s,c} = (4/3)\gamma_c^2 \nu_0 = 1.4 \times 10^{11} \text{Hz}$   $L_{\text{UV},45}^{-2} t_d^2 \beta_{0,-1}^4$ , and  $\nu_{s,m} = (4/3)\gamma_m^2 \nu_0 = 1.7 \times 10^{15} \text{Hz}$ .

### 3.2.2. Synchrotron radiation

Consider the synchrotron radiation by the shock-accelerated electrons, although it is not the dominant process of electron energy loss. In particular, we are interested in the synchrotron radiation contribution in the radio emission from SNe Ib/Ic Chevalier (1998); Björnsson & Fransson (2004). Define  $\nu_a$  as the frequency that synchrotron absorption optical depth is unity, and



the electron LF that emitting photons at  $\nu_a$  as  $\gamma_a$ . It should be noted, and confirmed later, that we are facing the problem with the minimum injection LF  $\gamma_m$  and the cooling LF  $\gamma_c$  being close to unity, and far smaller than  $\gamma_a$ , i.e.,  $\gamma_a \gg 1$  and  $\gamma_m \sim \gamma_c \sim 1$ . We still take broken power law approximation for the synchrotron spectrum.

The interested frequency range for GHz-radio emission would be the spectral segments around  $\nu_a$ , which, as derived in Appendix, is

$$\nu_a \approx 8.1 \text{GHz} t_d^{-\frac{p+3}{p+5}} L_{\text{UV},45}^{-\frac{2}{p+5}} A_{35}^{\frac{p+7}{2(p+5)}} \epsilon_{B,-1}^{\frac{p+3}{2(p+5)}} \beta_{0,-1}^{\frac{2}{p+5}} f_{\text{rel}}^{\frac{2}{p+5}}, \quad (11)$$

Either fast cooling  $\gamma_c < \gamma_m$  or slow cooling regime  $\gamma_m < \gamma_c$ , the synchrotron flux at  $\nu > \max(\nu_m, \nu_c)$  is given by

$$F_{\nu, \text{syn}} = \begin{cases} F_m \nu_m^{(p-1)/2} \nu_c^{1/2} \nu_a^{-(p+5)/2} \nu^{5/2}, & \nu < \nu_a \\ F_m \nu_m^{(p-1)/2} \nu_c^{1/2} \nu^{-p/2}, & \nu \geq \nu_a \end{cases} \quad (12)$$

where  $\nu_m$  and  $\nu_c$  are the characteristic frequencies emitted by electrons with LFs of  $\gamma_m$  and  $\gamma_c$ , respectively, and  $F_m = f_{\text{rel}} N_e P_m / 4\pi d_L^2$ , with  $P_m = \sqrt{3} e^3 B / m_e c^2$  being the synchrotron specific power of a single electron at its characteristic frequency  $\nu = 3\gamma_e^2 e B / 4\pi m_e c$ . Thus we can derive

$$F_m = 91 \mu\text{Jy} A_{35}^{3/2} \epsilon_{B,-1}^{1/2} d_{L,28}^{-2} \beta_{0,-1} f_{\text{rel}}. \quad (13)$$

If the CSM is dense and ionized or partially ionized, free-free absorption could be important for radio emission. The free-free absorption optical depth in a wind profile between radius  $R$  and observer is given by

$$\tau_{\text{ff}} \approx 0.16 T_{e,4}^{-1.35} A_{35}^2 \beta_{0,-1}^{-3} \nu_{10}^{-2.1} t_d^{-3}. \quad (14)$$

where  $T_e$  is the temperature of the electrons in the CSM (Lang 1999), and we take  $T_e = 2.0 \times 10^4 \text{K}$  below. The observed synchrotron flux after correction for free-free absorption should be  $F_\nu = F_{\nu, \text{syn}} \exp[-\tau_{\text{ff}}(\nu)]$ .

#### 4. PARAMETER CONSTRAINTS

We use the model described above to fit the X-ray and radio data of ASASSN-15lh. The X-ray data can be interpreted by IC radiation due to upscattering of the intense UV radiation. In order to calculate the IC radiation we need the UV light curve as input, thus we first fit the UV light curve with two connecting third-order polynomials,  $L_{\text{UV}} = a_3 t^3 + a_2 t^2 + a_1 t + a_0$ , with  $(a_3, a_2, a_1, a_0) = (3.95 \times 10^{-6}, -7.77 \times 10^{-4}, 3.44 \times 10^{-2}, 11.5)$  for  $t < 100$  days (rest frame time since explosion), and  $(2.77 \times 10^{-8}, -2.83 \times 10^{-5}, 6.30 \times 10^{-3}, 10.7)$  for  $t \geq 100$  days. Here  $L_{\text{UV}}$  is in unit of  $L_\odot$ , and  $t$  in day. This fitting function is shown in Fig. 1 as a red solid curve, in comparison with the UV data from Godoy-Rivera et al. (2017). With these seed photons, the calculated IC flux is also shown in Fig. 1. We have integrated the IC flux over the energy range of 0.3 – 10 keV to match the observed X-ray energy range. The IC luminosity is constant with time, well fitting the detected persistent X-ray flux (Table 1).

We explain why the IC flux is constant here. The X-ray emitting electrons are cooling fast due to upscattering the intense UV photons, so the X-ray range lies in a regime of  $\nu \gg \max(\nu_{s,m}, \nu_{s,c})$ . In this regime, no matter the

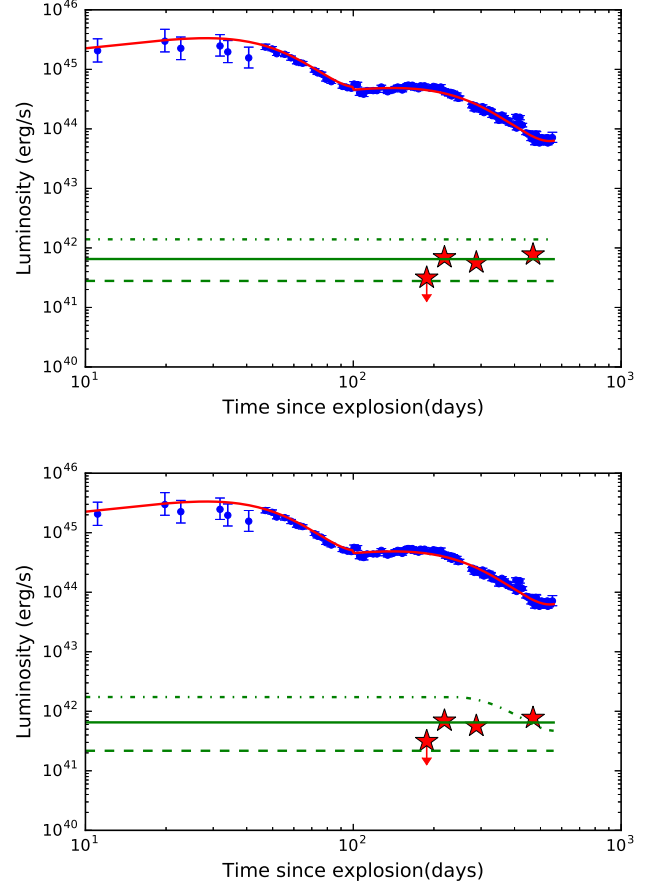


FIG. 1.— IC radiation light curve from upscatterings of UV photons in comparison with observations. The upper panel is for fixing  $\beta_0 = 0.03$ , whereas  $A_{38} = 0.3, 0.7$ , and  $1.5$  for dashed, solid and dashed-dotted lines, respectively. The lower panel is for fixing  $A_{38} = 0.7$ , whereas  $\beta_0 = 0.01, 0.03$ , and  $0.08$  for the green dashed, solid and dashed-dotted lines, respectively. The red stars are the X-ray data. The blue dots show the bolometric luminosity evolution, and the red solid line shows the fitting function. The other parameters used are  $\epsilon_e = 0.1$  and  $p = 3$ .

bulk electrons are fast or slow cooling (i.e.,  $\gamma_c < \gamma_m$  or  $\gamma_m < \gamma_c$ ), the IC flux is given by, see eqs. (9) and (10),  $F_{\nu, \text{IC}} = F_{m, \text{IC}} \nu_{s,m}^{(p-1)/2} \nu_{s,c}^{1/2}$ . During the evolution stage concerned, the SN-shock swept-up CSM material is not enough to decelerate the shock, and the shock keeps a constant velocity  $\beta \simeq \beta_0$ , hence the postshock electron's characteristic LF is also a constant, since  $\gamma_m \propto \beta^2$  or  $\gamma_m = 2$ . Thus  $\nu_{s,m} \propto \gamma_m^2$  is also a constant. Next, the total number of swept-up CSM electrons  $N_e \propto R \propto t$ , within which the fraction of relativistic electrons is also constant,  $f_{\text{rel}} = 1$  or  $\propto \beta^2$ , and the peak specific IC power is  $P_{m, \text{IC}} \propto U_{\text{ph}}$ , then the peak IC flux scales as  $F_{m, \text{IC}} \propto f_{\text{rel}} N_e P_{m, \text{IC}} \propto U_{\text{ph}} t$ . At last, the electron cooling LF  $\gamma_c \propto U_{\text{ph}} t$ , thus  $\nu_{s,c} \propto \gamma_c^2 \propto U_{\text{ph}}^2 t^{-2}$ . Putting all together we have  $F_{\nu, \text{IC}} \propto t^0$ , not changing with time. In short, a medium density with  $n \propto R^{-2}$  and IC radiation in the fast cooling regime, the IC flux is a constant. Actually, for  $\nu > \max(\nu_{s,m}, \nu_{s,c})$  we can derive

$$F_{\nu, \text{IC}} = 1.0 \times 10^{-8} \mu\text{Jy} A_{35} \beta_{0,-1} d_{L,28}^{-2} \gamma_m^{p-1} \nu_{18}^{-p/2} f_{\text{rel}}, \quad (15)$$

independent of time.

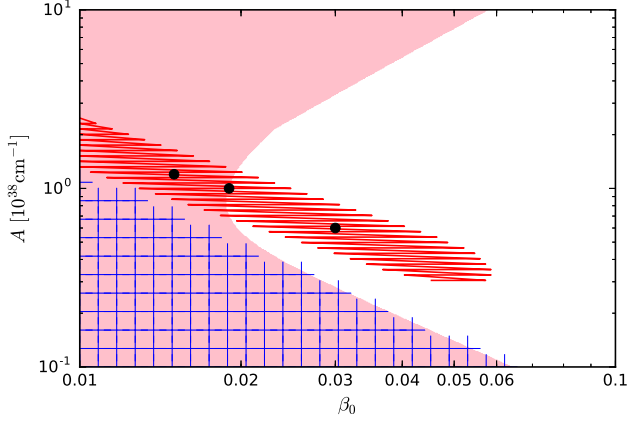


FIG. 2.— The parameter constraints in the  $(\beta_0, A)$  2D space with observations. The red oblique-line region shows the X-ray flux constraint. The blue grid (pink shaded) region show the constraints from 9 GHz upper limit, without (with) free-free absorption taken into account. The parameters used are:  $\epsilon_B = 0.1$ ,  $\epsilon_e = 0.1$ ,  $p = 3$  and  $T_e = 2.0 \times 10^4$  K.

The constant IC flux phase may end when the break  $\nu_{s,c}$  crosses the observing band. Letting  $\nu_{s,c} \simeq 10^{18}$  Hz we obtain that the crossing occurs at time

$$t_{\text{cross}} = 2.7 \times 10^3 \text{ days } L_{\text{UV},45} \beta_{0,-1}^{-2}. \quad (16)$$

After  $t_{\text{cross}}$  the X-ray band enters the regime of  $\nu_{s,c} > \nu > \nu_{s,m}$ , where the IC-produced flux at  $\sim 10^{18}$  Hz is  $F_{\nu, \text{IC}} \propto F_{m, \text{IC}} \propto U_{\text{ph}} t \propto L_{\text{UV}} t^{-1}$ , decreasing with time.

In order to constrain the parameters, we apply the least square fitting method to fit the persistent X-ray emission. We define  $\chi^2 = \sum_{i=1}^N (F_{\text{thy}}[i] - F_{\text{obs}}[i])^2$ , where  $F_{\text{thy}}$  is the theoretical value calculated by the IC radiation in Eq. (9) and Eq. (10),  $F_{\text{obs}}$  is the observed X-ray flux as presented in Table 1, and  $N$  is the total data number. We look for the minimum  $\chi^2$  value,  $\chi_{\text{min}}^2$ , in the  $(A, \beta_0)$  2D space, then constrain the parameters  $\beta_0$  and  $A_{38}$  in the 2D space by requiring  $\chi^2 < 2.0\chi_{\text{min}}^2$ . The resulted parameter region is showed in red in Fig. 2. We see that there is a relation between the constrained  $A$  and  $\beta_0$  values. Actually by equating the IC flux at  $\nu > \max(\nu_{s,m}, \nu_{s,c})$  (eq.15) and the observed X-ray flux we derive the  $A$ – $\beta_0$  relation,  $A_{38} \simeq 0.18\beta_{0,-1}^{-1} f_{\text{rel}}^{-1}$ . Moreover, the upper limit on  $\beta_0$  can be obtained by requiring  $t_{\text{cross}}$  larger than observed time of the last X-ray data,  $\beta_0 \lesssim 0.06$ .

The radio upper limits can further help to constrain the parameters. Fig 3 shows the synchrotron spectrum at 197 days in comparison with radio limits from observations. By requiring the synchrotron flux (Eq. 12) to satisfy the upper limit  $F_{\nu, \text{syn}} < 21 \mu\text{Jy}$  at 9 GHz at 197 days, we constrain the allowed region in the  $(A, \beta_0)$  space (Fig 2). Furthermore, by requiring the observed flux  $F_\nu = F_{\nu, \text{syn}} \exp[-\tau_{\text{ff}}(\nu)]$ , with free-free absorption taken into account, to satisfy the observed limit, the allowed parameter region is larger, as shown in Fig 2.

Combining the constraints by X-ray and radio observations, the allowed parameter ranges are  $A \gtrsim 10^{38} \text{ cm}^{-1}$ , and  $\beta_0 \lesssim 0.02$ , as shown in Fig. 2 the overlapping region between the X-ray constraint region (red-oblique-lined) and the radio constraint region (pink-shaded).

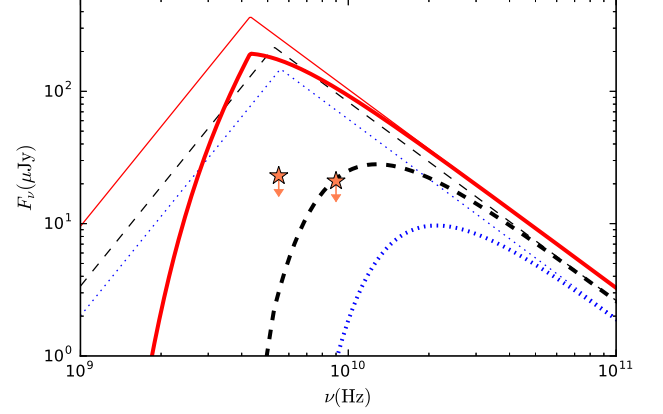


FIG. 3.— The model synchrotron spectrum in comparison with the radio limits from observations. The thick (thin) lines represent synchrotron flux with (without) free-free absorption taken into account. Three cases satisfying X-ray constraints are, as marked as black solid points in Fig. 2,  $(A_{38}, \beta_0) = (0.6, 0.03)$  (red solid lines),  $(1.0, 0.019)$  (black dashed lines), and  $(1.2, 0.015)$  (blue dotted lines), respectively. The other parameters used are:  $\epsilon_B = 0.1$ ,  $\epsilon_e = 0.1$ ,  $p = 3$  and  $T_e = 2.0 \times 10^4$  K.

## 5. CONCLUSIONS AND DISCUSSION

We have investigated the persistent X-ray emission from the location of ASASSN-15lh, and found that it can be produced by the SN shock propagating in a dense wind ( $n \propto R^{-2}$ ), where the shock-accelerated electrons emit the X-rays by upscattering the inner-coming UV photons from the SN photosphere. In this model we can constrain that the wind density parameter is  $A \gtrsim 10^{38} \text{ cm}^{-1}$ , and that the SN shock's initial velocity is  $v_{\text{sh}} < 0.02c$ . This  $A$  value corresponds to a stellar-wind's mass-loss rate of  $\dot{M} \geq 3 \times 10^{-3} M_\odot v_{w, \text{syr}}^{-1}$ , assuming a wind velocity of  $v_w = 10^8 \text{ cm s}^{-1}$ . The constrained SN shock velocity is somewhat lower compared to the average among the radio SNe,  $v_{\text{sh}}/c \approx 0.07$  (e.g., Kamble et al. 2016, and references there in).

With the constraints,  $A_{38}\beta_{0,-1} \sim 0.18$ , and  $\beta_0 \lesssim 0.02$ , we can calculate the shock energy (eq.2) at  $t \sim 500$  days,  $E \lesssim 2 \times 10^{49}$  erg, much smaller than the total radiation energy of ASASSN-15lh, and the typical kinetic energy of normal SNe. The shock radius at  $t \sim 500$  days is  $R = \beta_0 c t \lesssim 8 \times 10^{-3} \text{ pc}$ , within which the CSM mass is about  $M = 4\pi A m_p \beta_0 c t \sim 0.027 M_\odot$ . This mass should be ejected by the wind of ASASSN-15lh's progenitor within a time of  $R/v_w \lesssim 8 v_{w,8}^{-1}$  yrs before the SN explosion.

Recent-year observations of SN spectra within days of explosion have led to discovery of narrow emission lines in the early spectra of various kinds of SNe, indicating dense CSM immediately surrounding the progenitor stars. Gal-Yam et al. (2014) first reported detection of strong emission lines in a SN IIB's early spectrum, indicating a strong Wolf-Rayet-like wind with  $\dot{M} \sim 10^{-2} M_\odot \text{ yr}^{-1} (v_w/500 \text{ km s}^{-1})$ . More recently, Yaron et al. (2017) observed narrow emission lines from a regular type II SN, implying a dense wind of  $\dot{M} \sim 3 \times 10^{-3} M_\odot \text{ yr}^{-1} (v_w/100 \text{ km s}^{-1})$  ejected yrs before explosion. And the rapid spectra obtained within 5 days of SN II explosion have led to detection of narrow

emission lines in a significant fraction, 18%, of early spectra of SNe II (Khazov et al. 2016). These observations implies that dense winds may be common in core-collapse SNe. Our interpretation of X-ray emission from ASASSN-15lh may indicate that type I SLSNe are also surrounded immediately by a dense wind, ejected yrs be-

fore the SN explosion.

We thank Alexander Kann, Giorgos Leloudas, Tianqi Huang, Wenbin Lu, Yuanpei Yang, Yunwei Yu for helpful comments and discussions. This work is supported by the NSFC (No. 11773003) and the 973 Program of China (No. 2014CB845800).

## APPENDIX

### SYNCHROTRON SELF-ABSORPTION FREQUENCY

The radio band that is interested here is in the frequency regime of  $\nu \gg \max(\nu_c, \nu_m)$ . The electrons responsible to the radio emission are, due to fast cooling, distributed as  $dn_e/d\gamma_e = C\gamma_e^{-(p+1)}$  at  $\gamma_e(\nu) \gg \max(\gamma_c, \gamma_m)$ , where  $p$  is the index of injected electrons. Using  $\int_{\min(\gamma_c, \gamma_m)}^{\infty} (dn_e/d\gamma_e)d\gamma_e = 4nf_{\text{rel}}$ , we derive  $C \approx 4f_{\text{rel}}\gamma_c\gamma_m^{p-1}n$ . The absorption coefficient at  $\nu$  is given by (Rybicki & Lightman 1979)

$$\alpha_\nu = \frac{p+3}{8\pi m_e \nu^2} \int_{\gamma_{\text{obs}}} P(\tilde{\gamma}_e, \nu) C \tilde{\gamma}_e^{-p-2} d\tilde{\gamma}_e, \quad (\text{A1})$$

where the specific synchrotron power by an electron with  $\gamma_e$  is given by  $P(\gamma_e, \nu) = P_m(\nu/\nu_{\text{syn}}(\gamma_e))^{1/3}$ ,  $\nu_{\text{syn}} = 3\gamma_e^2 eB/4\pi m_e c$ , and  $\gamma_{\text{obs}} = (4\pi m_e c \nu/3eB)^{1/2}$ . Thus

$$\alpha_\nu = \frac{\sqrt{3}e^3}{8\pi m_e^2 c^2} \left( \frac{3e}{4\pi m_e c} \right)^{-1/3} \frac{p+3}{p+\frac{5}{3}} C B^{2/3} \nu^{-5/3} \gamma_{\text{obs}}^{-p-(5/3)} \quad (\text{A2})$$

$$= 1.68 \times 10^{26} \text{cm}^{-1} f_{\text{rel}} t_d^{-\frac{p+5}{2}} L_{\text{UV},45}^{-1} A_{35}^{\frac{p+7}{4}} \epsilon_{B,-1}^{\frac{p+3}{4}} \nu^{-\frac{p+5}{2}} \quad (\text{A3})$$

where in the second equation we have plugged in the expressions for  $C$ ,  $B$  and  $\gamma_{\text{obs}}$ , and the coefficient is calculated for  $p = 3$ . By setting the optical depth  $\tau \approx \alpha_\nu R/10 = 1$ , we obtain the absorption frequency

$$\nu_a \approx 8.1 \text{GHz} t_d^{-\frac{p+3}{p+5}} L_{\text{UV},45}^{-\frac{2}{p+5}} A_{35}^{\frac{p+7}{2(p+5)}} \epsilon_{B,-1}^{\frac{p+3}{2(p+5)}} \beta_{0,-1}^{\frac{2}{p+5}} f_{\text{rel}}^{\frac{2}{p+5}}. \quad (\text{A4})$$

## REFERENCES

- Björnsson, C.-I., & Fransson, C. 2004, *ApJ*, 605, 823  
 Chatzopoulos, E., Wheeler, J. C., Vinko, J., et al. 2016, *ApJ*, 828, 94  
 Chevalier, R. A. 1998, *ApJ*, 499, 810  
 Chevalier, R. A., & Fransson, C. 2006, *ApJ*, 651, 381  
 Chevalier, R. A., & Irwin, C. M. 2011, *ApJ*, 729, L6  
 Dai, Z. G., Wang, S. Q., Wang, J. S., Wang, L. J., & Yu, Y. W. 2016, *ApJ*, 817, 132  
 Dong, S., Shappee, B. J., Prieto, J. L., et al. 2016, *Science*, 351, 257  
 Gal-Yam, A., Mazzali, P., Ofek, E. O., et al. 2009, *Nature*, 462, 624  
 Gal-Yam, A. 2012, *Science*, 337, 927  
 Gal-Yam, A., Arcavi, I., Ofek, E. O., et al. 2014, *Nature*, 509, 471  
 Ghisellini, G. 2013, *Lecture Notes in Physics*, Berlin Springer Verlag, 873,  
 Godoy-Rivera, D., Stanek, K. Z., Kochanek, C. S., et al. 2017, *MNRAS*, 466, 1428  
 Kamble, A., Margutti, R., Soderberg, A. M., et al. 2016, *ApJ*, 818, 111  
 Kasen, D., & Bildsten, L. 2010, *ApJ*, 717, 245  
 Kool, E. C., Ryder, S. D., Stockdale, C. J., et al. 2015, *The Astronomer's Telegram*, 8388,  
 Khazov, D., Yaron, O., Gal-Yam, A., et al. 2016, *ApJ*, 818, 3  
 Krühler, T., Fraser, M., Leloudas, G., et al. 2017, *arXiv:1710.01045*  
 Lang, K. R. 1999, *Astrophysical Formulae* (New York: Springer)  
 Leloudas, G., Fraser, M., Stone, N. C., et al. 2016, *Nature Astronomy*, 1, 0002  
 Margutti, R., Metzger, B. D., Chornock, R., et al. 2017, *ApJ*, 836, 25  
 Metzger, B. D., Margalit, B., Kasen, D., & Quataert, E. 2015, *MNRAS*, 454, 3311  
 Nicholl, M., Smartt, S. J., Jerkstrand, A., et al. 2014, *MNRAS*, 444, 2096  
 Piran, T., Nakar, E., & Rosswog, S. 2013, *MNRAS*, 430, 2121  
 Quimby, R. M., Aldering, G., Wheeler, J. C., et al. 2007, *ApJ*, 668, L99  
 Rybicki, G. B., & Lightman, A. P. 1979, *New York, Wiley-Interscience*, 1979. 393 p.,  
 Sari, R., Piran, T., & Narayan, R. 1998, *ApJ*, 497, L17  
 Sironi, L., & Giannios, D. 2013, *ApJ*, 778, 107  
 Smith, N., & McCray, R. 2007, *ApJ*, 671, L17  
 Walch, S., & Naab, T. 2015, *MNRAS*, 451, 2757  
 Woosley, S. E., Blinnikov, S., & Heger, A. 2007, *Nature*, 450, 390  
 Woosley, S. E. 2010, *ApJ*, 719, L204  
 Woosley, S. E. 2017, *ApJ*, 836, 244  
 Yaron, O., Perley, D. A., Gal-Yam, A., et al. 2017, *Nature Physics*, 13, 510